# Barocaloric Properties of Quaternary $Mn_3(Zn,In)N$ for Room Temperature Refrigeration Applications

David Boldrin,[1,2,*] Eduardo Mendive-Tapia,[3,4] Jan Zemen,[5] Julie B. Staunton,[3] Angelo M. Gomes,[6] Luis Ghivelder,[6] John Halpin,[2] Alexandra Gibbs,[7] Araceli Aznar,[8] Josep-Lluís Tamarit,[8] Pol Lloveras,[8] Xavier Moya,[9] and Lesley F. Cohen[1]

[1] *Department of Physics, Blackett Laboratory, Imperial College London, London, SW7 2AZ, UK*
[2] *School of Physics and Astronomy, University of Glasgow, Glasgow, UK*
[3] *Department of Physics, University of Warwick, Coventry CV4 7AL, United Kingdom*
[4] *Department for Computational Materials Design, Max-Planck-Institut für Eisenforschung, 40237 Düsseldorf, Germany*
[5] *Faculty of Electrical Engineering, Czech Technical University in Prague, Technická 2, Prague 166 27, Czech Republic*
[6] *Instituto de Fisica, Universidade Federal do Rio de Janeiro, 21941-972 Rio de Janeiro, RJ, Brazil*
[7] *ISIS Facility, Rutherford Appleton Laboratory, Chilton, Didcot OX11 0QX, United Kingdom*
[8] *Departament de Física, EEBE, Campus Diagonal-Besòs and Barcelona Research Center in Multiscale Science and Engineering, Universitat Politècnica de Catalunya, Eduard Maristany, 10-14, 08019 Barcelona, Catalonia, Spain*
[9] *Department of Materials Science, University of Cambridge, Cambridge CB3 0FS, United Kingdom*

(Dated: August 26, 2021)

The magnetically frustrated manganese nitride antiperovskite family display significant changes of entropy under hydrostatic pressure that can be useful for the emerging field of barocaloric cooling. Here we show that barocaloric properties of metallic antiperovskite Mn nitrides can be tailored for room temperature application through quaternary alloying. We find an enhanced entropy change of $\Delta S_t = 37\,\mathrm{J\,K^{-1}\,kg^{-1}}$ at the $T_t = 300\,\mathrm{K}$ antiferromagnetic transition of quaternary $Mn_3Zn_{0.5}In_{0.5}N$ relative to the ternary end-members. The pressure-driven barocaloric entropy change of $Mn_3Zn_{0.5}In_{0.5}N$ reaches $\Delta S_{\mathrm{BCE}} = 20\,\mathrm{J\,K^{-1}\,kg^{-1}}$ in 2.9 kbar. Our results open up a large phase space where new compounds with improved barocaloric properties may be found.

## INTRODUCTION

The field of caloric cooling offers opportunities for greater energy-efficient refrigeration without the need for environmentally harmful fluids. Magnetocalorics and electrocalorics are by far the most studied phenomena, with continued significant advances [1] although as yet without wide commercial uptake. Mechanocalorics including baro- and elastocalorics are only beginning to gain prominence [2, 3] in part due to the perceived device engineering challenges combined with the relatively small range of materials displaying large mechanocaloric effects, particularly for barocalorics, the majority of which show large hysteresis. However, concerted efforts stimulated by significant increases in elastocaloric effects have recently led to design breakthroughs [4]. Driven by the ever-increasing magnitude of the barocaloric effects (BCE) reported [5, 6], similar developments can be envisaged for a barocaloric device and have indeed recently been patented [7].

Manganese nitride antiperovskites ($Mn_3AN$) display a number of unusual properties, such as an anomalous coefficient of resistivity [8], negative thermal expansion [9], and piezomagnetism [10]. Recently, giant BCE have been reported in the $A$ = Ga and Ni members of the family [10, 11]. These effects originate from a non-collinear antiferromagnetic (AFM) order born from frustrated spin interactions, which strengthen with changes of volume and via feedback with the underlying electronic structure as magnetic order develops [10]. Both magnetovolume effects and the feedback with the electronic structure leads to a complex and rich mechanism that underpins the strongly 1$^{\mathrm{st}}$-order paramagnetic to AFM transition and, hence, the giant BCE properties [10]. As metals, their large density (important for compact applications) and high thermal conductivity (important for heat exchange) offer two important advantages for barocalorics over e.g. ceramics and plastic crystals.

This work sets out to exploit the $Mn_3(A,B)N$ family's chemical flexibility, where the $(A,B)$ site can be taken up by many transition and post-transition metals. We are motivated to investigate the effect of quaternary alloying on the barocaloric properties. The study is particularly pertinent given our recent observation of unexpectedly large barocaloric effects in $Mn_3NiN$, given the relatively small transitional volume change, originating from multisite magnetic exchange [10]. Moreover, quaternary alloying presents an ideal route to tailor the transition temperature, $T_t$, for refrigeration applications close to room temperature; $A$ = Sn, Ge, In and Pd all have $T_t$ above 300 K, whilst the remainder ($A$ = Zn, Co, Ag, Ni, Rh, Cu…) lie below [9]. We study $Mn_3Zn_{1-x}In_xN$, where $T_t$ (Zn, $x = 1$) = 180 K and $T_t$ (In, $x = 0$) = 380 K, using dilatometry and temperature and pressure dependent neutron diffraction, magnetometry and calorimetry measurements. We show that $Mn_3Zn_{0.5}In_{0.5}N$ undergoes a magnetic transition at $T_t$= 300 K with a concurrent volume change $\frac{\Delta V_t}{V} = 0.9\,\%$. This transition temperature

decreases with pressure, $\frac{dT_t}{dp} = -3.3\,\mathrm{K\,kbar^{-1}}$, meaning the operational temperature is ideal for air conditioning. We find that $\frac{\Delta V_t}{V}$ is larger than expected in this material based on the sensitivity of $T_t$ to pressure, $\frac{dT_t}{dp}$. Using the same framework we previously used to analyse $Mn_3NiN$, we show that multi-site magnetic exchange terms appear responsible for the enhanced 1$^{st}$-order nature of the transition in this material. The transitional entropy change of $\Delta S_t = 37\,\mathrm{J\,K^{-1}\,kg^{-1}}$ estimated from the Clausius-Clapeyron relation at zero pressure is larger than both the ternary end-members and $Mn_3GaN$ [11], whilst the pressure-driven barocaloric entropy change reaches $20\,\mathrm{J\,K^{-1}\,kg^{-1}}$ in 2.9 kbar. When normalising by volume $\Delta S_t = 0.25\,\mathrm{J\,K^{-1}\,cm^{-3}}$, which is comparable to the colossal BCE close to room temperature recently found in plastic crystals, 0.42 and $0.48\,\mathrm{J\,K^{-1}\,cm^{-3}}$ for NPG and MNP (2-methyl-2-nitro-1-propanol), respectively [6], due to the $\sim 7$ times larger density in the former. These results evidence the rich chemical phase space provided by $Mn_3(A,B)N$ that allow fine tuning of the transition temperature and can lead to unexpected enhancement of their barocaloric properties.

## EXPERIMENTAL

Samples were prepared using a standard solid state synthesis technique. Firstly, $Mn_2N_{0.86}$ was prepared as detailed in Ref. [12]. Subsequently, the $Mn_2N_{0.86}$ precursor was ball-milled and then thoroughly mixed by hand with elemental Zn (Sigma-Aldrich, 99.9 % purity, 150 $\mu$m) and/or In powder (Sigma Aldrich, 99.99% purity). The resulting mixture was pressed into $\sim$2 g pellets, wrapped in Ta foil and sealed in evacuated quartz ampoules. The ampoules were heated to 780°C for 2 days before being furnace cooled to room temperature. The regrinding, pelletisation and reaction steps were repeated if X-ray diffraction showed starting reagents to still be present.

Thermal expansion measurements were made with a silver based capacitance dilatometer [13] fitted in a PPMS system (manufactured by Quantum Design, Inc.). SEM-EDS and EBSD was performed using a Helios dual column plasma FIB-SEM.

Neutron diffraction was performed at the HRPD beamline at the ISIS neutron source, UK. Pressure dependent measurements were performed using a TiZr gas high-pressure cell. Data were also collected in a standard vanadium slab can on the same sample.

Pressure dependent calorimetry measurements were performed using two different Cu-Be high-pressure cells that can operate in the temperature range $210 - 393$K, controlled by an external thermal bath. One is a MV1-30 cell (Unipress, Poland) adapted as a differential thermal analyser by means of Peltier modules as thermal sensors, and that can operate in the pressure range 0−6 kbar. The other is a custom-built cell that uses Bridgman thermocouples as thermal sensors and that can operate in the pressure range $0 - 3$ kbar. The sample was mixed with a perfluorinated fluid (Galden Bioblock Scientist) and encapsulated in a tin capsule. The pressure-transmitting fluid was DW-Therm M90.200.02 (Huber GmbH). Construction of the isobaric entropy-temperature curves is described in the supplementary information (S.I.).

## RESULTS AND DISCUSSION

We begin by characterising the crystal and magnetic structures of $Mn_3Zn_{0.5}In_{0.5}N$ before turning to measurements of the barocaloric properties of $Mn_3Zn_{1-x}In_xN$($x$ = 0, 0.5 and 1). We performed neutron diffraction measurements on the former as a function of temperature and applied pressure. Data were collected between 10 and 312 K at ambient pressure and between 0 and 5.4 kbar at 294 K on the HRPD beamline at ISIS, UK. Rietveld refinement of the data collected at 10 K is shown in Figure 1a and was performed using the Fullprof [14] and GSAS2 [15] software packages. Away from the transition region, the data is well fitted by a single antiperovskite phase with $Pm\bar{3}m$ symmetry and lattice parameter $a = 3.9475$ Å at 10 K. Due to the close neutron scattering lengths of Zn and In ($b_{Zn} = 5.68$ and $b_{In} = 4.065 - 0.0539i$ fm), combined with the significant absorption from In, the occupancies on this crystallographic site would not refine stably. However, the sharpness of the peaks demonstrates that the sample is highly crystalline with a well-defined stoichiometry. No improvement to the fit was observed when allowing the Mn or N site occupancy to refine. The magnetic Bragg peaks at 10 K are aligned with the nuclear peaks, meaning the magnetic propagation vector is $k = 0$. The magnetic peaks are refined well with the non-collinear AFM $\Gamma^{5g}$ structure, using the notation of Fruchart et al. [16], with a moment size of 2.49 $\mu_B$ on each Mn site. Data collected on warming show no clear sign of a magnetic transition, evidenced by the temperature dependence of the (100) peak intensity in Figure 1b, until $T_N$ where all magnetic Bragg peaks disappear. The same magnetic structure is found in $Mn_3ZnN$ [17] (at high temperature), whilst it has also been proposed in $Mn_3InN$ [18]. It is therefore clear that in this case alloying preserves the $\Gamma^{5g}$ structure and does not induce competition with any additional magnetic phases.

Measurements performed as a function of temperature and pressure across the PM to AFM transition reveal the presence of regions where both phases exist. Figure 1c shows the temperature dependence of the (321) reflection intensity close to $T_N$ and highlights the coexistence of 2 peaks which originate from the PM and AFM states of the sample (See Figure S2 for the equivalent line plots). This is clear evidence that the transition does not pro-

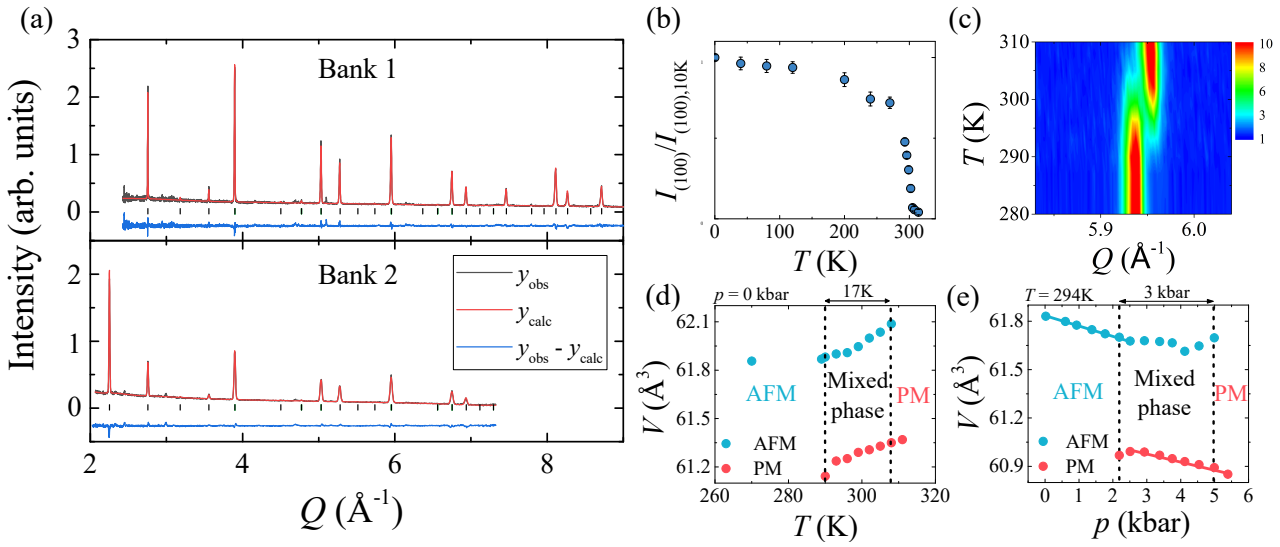


FIG. 1. (a) Rietveld refinement of powder neutron diffraction data collected at 10 K on banks 1 (back-scattering) and 2 (90°) of HRPD, ISIS. Black tick marks indicate the reflections from the antiperovskite phase. The minor additional peaks, *e.g.* at $Q = 5.1$ Å$^{-1}$, are from MnO; (b) Temperature dependence of the fitted (100) peak intensity. (c) Thermodiffractogram of the (321) reflection; (d) Temperature dependence of the lattice volume at ambient pressure close to $T_t$ for both the AFM and PM states; (e) Pressure dependence of the lattice volume at 294 K. Dotted vertical lines in (d) and (e) separate the single and mixed phase magnetic regimes, as described in the text. Solid lines in (e) are guides to the eye. Error bars in (d-e) are smaller than the symbol size.

ceed uniformly throughout the sample and therefore a mixed phase region exists. We fitted both phases (PM and AFM) in the transition region using a le Bail technique to determine the volume change of each, shown in Figure 1d. The region in which both phases exist is 17 K between 290 and 307 K and the volume change of the individual phases within this region behaves almost linearly, as is expected. Interestingly, the lattice expansion of the AFM phase in the transition region is significantly larger than both the pre-transitional region below 290 K and that of the PM phase within the transition region. Such behaviour hints at anomalous contributions to the transition, such as an elastic instability.

The mixed phase region can also be mapped out when the transition is driven by pressure, with a width of 3 kbar, from the AFM to PM state. Figure 1e shows the isothermal volume change of both AFM and PM phases as a function of pressure at $T = 294$ K, again determined using a le Bail fitting. According to Figure 1d, at this temperature the sample should be in the mixed phase region, however the diffraction data clearly shows that only the AFM phase is present (see Fig. S2c-d). This suggests a slight discrepancy between the temperature recorded in the standard sample holder and the pressure cell. Up until 2 kbar the volume of the AFM phase decreases linearly, as expected. Between 2 and 5 kbar, the PM phase appears and coexists with the AFM phase. The PM and AFM phases behave quite differently within the mixed phase region. The PM phase volume decreases linearly with increasing pressure. However, the AFM phase volume remains essentially constant between 2 and 4 kbar and increases sharply at pressures above this. Although we were unable to refine the magnetic structure from the data due to the large background from the pressure cell, the sharp change in volume of the AFM phase above 4 kbar strongly suggests that a magnetic transition occurs in this region and therefore that the $\Gamma^{5g}$ structure is unstable to pressure. Nonetheless, the phase coexistence in both the pressure and temperature dependent measurements are evidence of the ~~strongly~~ 1$^{st}$-order behaviour at the transition and suggest the presence of a barocaloric effect.

Moving to the barocaloric properties of the $x = 0$, 0.5 and 1 samples, we use the entropy change across the transition estimated using the Clausius-Clapeyron relation to compare between these and other antiperovskites. The relation is:

$$\Delta S_t^{CC} = \Delta V_t \left(\frac{dT_t}{dp}\right)^{-1} \quad (1)$$

where $\Delta S_t^{CC}$ is the entropy change from the Clausius-Clapeyron relationship, $\Delta V_t$ is the volume change at the transition and $\frac{dT_t}{dp}$ is the rate of change of the transition temperature, $T_t$ with applied pressure, $p$. This provides a useful figure of merit (FOM) to allow comparison of BCE between similar materials (assuming the similar volumes of $Mn_3AN$ and other metallic materials) given by FOM $= \frac{\Delta V_t}{V}\left(\frac{dT_t}{dp}\right)^{-1}$ [11]. This FOM evaluates how

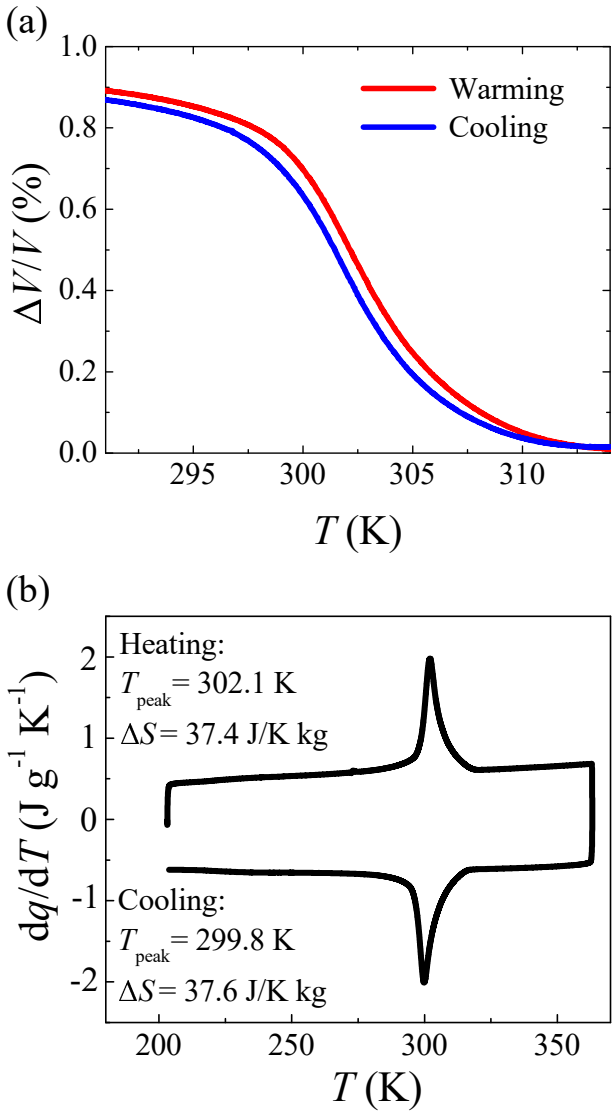


FIG. 2. (a) The volume change of $Mn_3Zn_{0.5}In_{0.5}N$ as a function of temperature measured using dilatometry. (b) Temperature dependent heat flow measurements at normal pressure.

large the discontinuity at the 1st-order PM-to-triangular AFM transition is, which directly relates to the size of the BCE.

As explained by Bean and Rodbell [19], the 1st-order character of a magnetic phase transition, and its magnitude, from the PM state to another ordered magnetic state can be attributed to the presence of an overall negative 4th-order coefficient in a Gibbs free energy, $G$ (expanded in terms of a magnetic order parameter), caused by a magnetovolume coupling in magnetic materials. We have previously shown that magnetic exchange correlations between the local moments that are higher order than pairwise, *i.e.* multisite interactions, can also generate an overall negative 4th-order contribution in the free energy, thus driving and enhancing the 1st-order character of the magnetic phase transition in $Mn_3AN$ [10]. As the electronic structure transforms as a response to different underlying states of magnetic order (e.g. paramagnetic, triangular antiferromagnetic, partially ordered, etc.), it produces a feedback on the magnetic interactions between the local moments. This means that different effective pairwise interactions would be obtained when calculated in different states of magnetic order. In other words, the interactions among the local moments in a material all the way from its paramagnetic state at high $T$ down to the low temperatures where the magnetic order is complete can thus be succinctly expressed in terms of pair and higher order multisite interactions. This effect is purely electronic in origin and can arise together with or in the absence of a magnetostructural coupling [20].

We determine the effect of both magnetovolume coupling and of multisite interactions by studying $G$ containing a hierarchy of local moment correlations, *i.e.* 2nd- and higher-order free energy magnetic terms [20]. The form of $G$ here emerges from previous first-principles studies of frustrated AFM materials and other magnetic systems at finite-temperature [10, 20–22]. However, in this work we extract the coefficients of $G$ instead from our experimental data as described in Ref. [10]. Our theoretical approach allows us to distinguish magnetovolume and purely electronic mechanisms ~~giving rise to multisite interactions~~, and their effect on the magnetic phase transition:

$$\begin{aligned} G = &- \mathcal{S}^{(2)}\left(M_1^2 + M_2^2 + M_3^2\right) - \mathcal{S}^{(4)}\left(M_1^4 + M_2^4 + M_3^4\right) \\ &- c_{\mathrm{mv}}\frac{\Delta V_{\mathrm{t}}}{V}\left(M_1^2 + M_2^2 + M_3^2\right) \\ &+ \frac{1}{2}\gamma\frac{\Delta V_{\mathrm{t}}^2}{V} + \Delta V_{\mathrm{t}} p - T S_{\mathrm{tot}} \end{aligned} \tag{2}$$

where $\mathcal{S}^{(2)}$ contains the effect of pairwise interactions, $\mathcal{S}^{(4)}$ arises from quartic multi-site contributions, $M_i$ is the magnetic order parameter, $c_{\mathrm{mv}}$ is the lowest order possible magnetovolume coupling, $\Delta V_{\mathrm{t}}$ is the volume change at the transition, $V$ is the volume of the unit cell in the paramagnetic state, $\gamma$ is the bulk modulus and $S_{\mathrm{tot}}$ is the total entropy coming from orientational magnetic degrees of freedom [20]. We highlight that the number of free energy coefficients has been reduced to the lowest possible by exploiting symmetry arguments of this crystal structure. The magnitudes of $\mathcal{S}^{(2)}$, $\mathcal{S}^{(4)}$, and $c_{\mathrm{mv}}$ are obtained by performing a fitting of the experimental values of $T_{\mathrm{N}}$, $\frac{\mathrm{d}T_{\mathrm{t}}}{\mathrm{d}p}$ , and $\Delta S$ (or the spontaneous volume change) to the corresponding predicted values of these quantities obtained after minimizing Equation 2 with respect to $M_i$ [10]. Albeit the fitting of these three parameters is done simultaneously, we highlight that the magnitudes of $\mathcal{S}^{(2)}$ and $c_{\mathrm{mv}}$ are mainly given by $T_{\mathrm{N}}$ and $\frac{\mathrm{d}T_{\mathrm{t}}}{\mathrm{d}p}$ , respectively, while $\mathcal{S}^{(4)}$ depends on the overall effect of the total 4th-order contribution in $G$, including that from $c_{\mathrm{mv}}$ , giving

rise to the 1st-order character and the size of the BCE. The value of the bulk modulus, $\gamma \sim 130\,\mathrm{GPa}$, is taken directly from experiment [9] and $S_{\mathrm{tot}}$ follows an analytical expression in terms of $M_i$ only, which is derived from a mean-field theory [20, 23]. Minimising equation 2 with respect to $\frac{\Delta V_{\mathrm{t}}}{V}$ gives $\frac{\Delta V_{\mathrm{t}}}{V} = \frac{c_{\mathrm{mv}}}{V\gamma}(M_1^2+M_2^2+M_3^2)-\frac{p}{\gamma}$, which substituted into equation 2 shows how the magnetovolume coupling generates a 4th-order free term on $M_i$ [10]. It is therefore apparent that either magnetovolume coupling, $c_{\mathrm{mv}}$ , or multi-site interactions, $\mathcal{S}^{(4)}$, can drive the 1st-order transition [10] since they generate 4th-order free energy coupling [19]. We previously found that the multi-site interactions enhance 1st-order character in $Mn_3NiN$, relative to $Mn_3GaN$, despite a smaller $\frac{\mathrm{d}T_{\mathrm{t}}}{\mathrm{d}p}$ and magnetovolume coupling [10]. The values of these interactions, $\mathcal{S}^{(4)}$, are given in Table 1, where being positive (negative) generates a negative (positive) total contribution in $G$ and therefore acts to stabilise (destabilise) the triangular AFM structure. We find for $Mn_3ZnN$ the 1st-order behaviour is largely driven by magnetovolume coupling as $c_{\mathrm{mv}}$ is large and $\mathcal{S}^{(4)}$ is negative. For $Mn_3InN$, the magnetovolume coupling is significant and $\mathcal{S}^{(4)}$ is positive, however the small volume change means the entropy change, $\Delta S_{\mathrm{t}}^{\mathrm{CC}}$, is also small.

We now turn to the pertinent results recorded in Table 1 on the $x = 0.5$ sample of the series $Mn_3Zn_{1-x}In_xN$. Figure 2a shows the volume as a function of temperature measured using dilatometry which demonstrates a large volume increase of $\frac{\Delta V_{\mathrm{t}}}{V} = 0.9\,\%$ at the PM-AFM transition, $T_{\mathrm{N}} \sim 300\,\mathrm{K}$. This volume change also leads to a large spontaneous magnetostriction, $\omega_{\mathrm{s,10K}}$ (see Table 1), a property that has previously been used to characterise $Mn_3AN$ [9]. The value reported here is of similar magnitude to the largest values found in $A$ = Zn and Ga. The heat flow data shown in Figure 2b gives an entropy change at the transition of $\Delta S_{\mathrm{t}} = 37.4 \pm 0.2$ and $37.6 \pm 0.2\,\mathrm{J\,K^{-1}\,kg^{-1}}$ on warming and cooling, respectively. The linear dependence of $T_{\mathrm{N}}$ with pressure measured using pressure dependent calorimetry gives $\frac{\mathrm{d}T_{\mathrm{t}}}{\mathrm{d}p} = -3.3 \pm 0.2\,\mathrm{K\,kbar^{-1}}$. This allows us to estimate the entropy change at the transition using the Clausius-Clapeyron relation, which gives a value of $\Delta S_{\mathrm{t}}^{\mathrm{CC}} = 37 \pm 2\,\mathrm{J\,K^{-1}\,kg^{-1}}$ in excellent agreement with the measured $\Delta S_{\mathrm{t}}$. Using the same method described for the ternary end-members, we also extracted $c_{\mathrm{mv}}$ and $\mathcal{S}^{(4)}$ for the $x = 0.5$ compound by minimising Equation 2 as explained above.

We can now make some comparisons between the ternary end-members and the quaternary sample. It is clear that the magnitude of the transitional volume change of the quaternary sample lies roughly in between the two end-members, suggesting a linear relationship of $\frac{\Delta V_{\mathrm{t}}}{V}$ on alloying. The behaviour of $\frac{\mathrm{d}T_{\mathrm{t}}}{\mathrm{d}p}$ is quite different as it is roughly the same for the $x = 0.5$ and 1 samples, whereas it is significantly larger for the $x = 0$. Given the behaviour of these two parameters, the resulting $\Delta S_{\mathrm{t}}^{\mathrm{CC}}$ after applying Equation 1 is significantly larger for the $x = 0.5$ sample compared to the end-members. These results clearly demonstrate that unexpected enhancements in the 1st-order nature of the transition can be achieved through quaternary alloying.

As expected from the $\frac{\mathrm{d}T_{\mathrm{t}}}{\mathrm{d}p}$ values, the magnetovolume coupling, $c_{\mathrm{mv}}$ , is similar for the $x = 0.5$ and 1 samples whereas it is significantly larger for the $x = 0$. Interestingly, a similar behaviour is found for $\mathcal{S}^{(4)}$; the value is positive for $x = 0.5$ and 1 whereas it is large and negative for $x = 0$. The overall effect of the multi-site Mn spin interactions, described by $\mathcal{S}^{(4)}$, is to stabilise (or destabilise) the non-collinear AFM structure for defined positive (or negative) values of $\mathcal{S}^{(4)}$. We previously found that these interactions enhance 1st-order character in $Mn_3NiN$ and produce a large transitional volume change relative to the magnetovolume coupling [10], evidenced by the large FOM, $\frac{\Delta V_{\mathrm{t}}}{V}\left(\frac{\mathrm{d}T_{\mathrm{t}}}{\mathrm{d}p}\right)^{-1}$, in Table 1. For $Mn_3Zn_{0.5}In_{0.5}N$ this ratio is similar to $Mn_3NiN$ and indeed both have positive $\mathcal{S}^{(4)}$ terms, suggesting the multi-site magnetic exchange plays an important role in enhancing the 1st-order transition in both. For $Mn_3ZnN$ this ratio is of similar magnitude to $Mn_3GaN$ and both have negative $\mathcal{S}^{(4)}$, which implies that magnetovolume coupling drives the 1st-order transition. For $Mn_3InN$ this ratio is significantly smaller than all other samples yet its $\mathcal{S}^{(4)}$ term is positive. This may stem from the larger transition temperature, $T_{\mathrm{t}} = 380\,\mathrm{K}$, meaning that the effect of $\mathcal{S}^{(4)}$ is comparatively smaller compared to $Mn_3Zn_{0.5}In_{0.5}N$. Further work on $Mn_3InN$ is required to make an accurate comparison, for instance by determining whether the same non-collinear AFM structure is present.

We now focus on the pressure driven barocaloric effects of $Mn_3Zn_{0.5}In_{0.5}N$. In Figure 3a-b, we show heat flow data measured as a function of temperature at different pressures. Integration of the heat flow data at different pressures allows us to construct isobaric entropy curves as shown in Figure 3c-d (see S.I. for a full description). The latter is used to determine the barocaloric entropy change, $\Delta S_{\mathrm{BCE}}$ (Figures 3e-f), and adiabatic temperature change, $\Delta T_{\mathrm{AD}}$ (Figures 3g-h), for a given pressure across the transition, using quasi-direct methods as previously described elsewhere [10]. We find that the magnitude of $\Delta S_{\mathrm{BCE}}$ and $\Delta T_{\mathrm{AD}}$ are significantly larger when measured on cooling than on warming, however the cause of this is unclear. At the highest applied pressure (4.2 kbar) the maximum on cooling of $\Delta S_{\mathrm{BCE}} = 22 \pm 3\,\mathrm{J\,kg^{-1}\,K^{-1}}$ and $\Delta T_{\mathrm{AD}} = 8.5 \pm 1\,\mathrm{K}$. Whilst in principle $\Delta S_{\mathrm{BCE}}$ should be similar to $\Delta S_{\mathrm{t}}$, the former is less than $\Delta S_{\mathrm{t}}$ (indicated in table 1) due to broadening of the transition, with the sharp 1st-order like change ~~close to the transition~~ giving a reduced entropy change $\Delta S_{\mathrm{t,1}} = 26.3\,\mathrm{J\,kg^{-1}\,K^{-1}}$ (see Figure S1). This latter number is in good agreement with $\Delta S_{\mathrm{BCE}}$ from our quasi-direct

TABLE I. Properties of various $Mn_3AN$ materials relevant to their barocaloric effects. $\omega_{s,10K}$ is the spontaneous magnetostriction at 10 K between the PM and AFM states. † The volume change is given by $\frac{\Delta V_t}{V} = 3^* \frac{dL}{L}$, where $\frac{dL}{L}$ is taken from [9]. * Obtained through the neutron diffraction data

| $A$ | $T_N$ (K) | $\frac{\Delta V_t}{V}$ (%) | $\frac{dT_t}{dp}$ ($K\,kbar^{-1}$) | $\frac{\Delta V_t}{V}\left(\frac{dT_t}{dp}\right)^{-1}$ ($\%\,kbar\,K^{-1} \times 10^{-1}$) | $\omega_{s,10K}$ (%) | $\Delta S_t^{CC}$ ($J\,K^{-1}\,kg^{-1}$) | $\Delta S_t$ ($J\,K^{-1}\,kg^{-1}$) | $c_{mv}$ (meV) | $\mathcal{S}^{(4)}$ (meV) |
|---|---|---|---|---|---|---|---|---|---|
| Ni [10] | 262 | 0.4 | -1.3 | 3.1 | 0.8 | 47 | 47 | 250 | 13 |
| Ga [9, 11] | 288 | 1.0 | -6.5 | 1.5 | 2.0 | 22 | 22 | 1107 | -25 |
| Zn | 186 | 1.5 [9]† | -7.0 | 2.1 | 2.0 [9] | 32 | 39 [24] | 1267 | -40 |
| $Zn_{0.5}In_{0.5}$ | 300 | 0.9 | -3.3 | 2.9 | 1.8* | 37 | 37 | 600 | 6 |
| In | 380 | 0.3 [9]† | -3.5 | 0.9 | 0.9 [9] | 12 | - | 650 | 6 |

BCE measurements (see Figure 3e), and it is expected that the two values would be in closer agreement at higher pressures as $\Delta S_{BCE}$ is not saturated at 4.2 kbar. ~~Moreover,~~ Consistently, the phase coexistence region between $290 < T(K) < 308$ in the neutron diffraction data roughly aligns with the sharp region ~~of the latent heat~~ in the heat flow data, corresponding to the 1st-order transition ~~further evidencing that only a part of the transition is strongly 1st-order~~. To attempt to better understand the origin of this pre-transitional region, we performed SEM-EDX compositional analysis combined with EBSD. The data show a partial segregation of In to grain boundaries (see Figure S3) leaving the grain centres Zn rich (see Table S1). The sharpness of the neutron diffraction peaks demonstrates that the sample does not consist of a range of stoichiometries with varying Zn/In ratios, and therefore it appears this segregation is limited to a small volume percent of the sample at the grain boundary region. Nonetheless it may explain the increased pre-transitional region of the transition. Further reaction steps, in an attempt to homogenise the sample, did not lead to stronger 1st-order behaviour.

We now discuss the observed properties of $Mn_3Zn_{0.5}In_{0.5}N$ in the context of other studies of quaternary alloying in this antiperovskite family. Anomalous behaviour in $Mn_3(A,B)N$ materials obtained by quaternary alloying has previously been demonstrated and related to the geometrically frustrated nature of the nearest-neighbour AFM interactions. For instance, it was previously observed that in the $Mn_3(Cu_{1-x},Ge_x)N$ and $Mn_3(Cu_{1-y},Sn_y)N$ series increased $x$ or $y$ doping (i) induces unexpectedly large $\frac{\Delta V_t}{V}$ compared to the end members and (ii) reduces the volume of the PM state [9]. This was proposed to arise from strong magnetovolume coupling of the frustrated AFM interactions, which assists lattice contraction and reduces the PM lattice volume as well as suppressing the spin fluctuations in the PM phase. In particular, in the case of $Mn_3GaN$ Matsunami *et al.* concluded that the giant BCE is attributable to such a magnetically frustrated mechanism principally owing to the strong magnetovolume coupling enhancing the change of volume with pressure [11], in agreement with our findings.

Our results show that magnetic frustration generates a more complex origin for the giant BCEs in antiperovskite materials. As we previously found for $Mn_3NiN$, the higher order multi-site exchange effects, captured by $\mathcal{S}^{(4)}$, add to the effect of magnetovolume coupling to enhance the 1st-order character in $Mn_3Zn_{0.5}In_{0.5}N$. Both of these stem directly from the geometrically frustrated magnetism. In addition, the presence of $\mathcal{S}^{(4)}$ and its stabilising effect on the AFM structure allows $\frac{dT_t}{dp}$ to remain small relative to the large discontinuity at the magnetic phase transition, with an associated larger BCE. Taken together, alloying has produced an entropy change larger than anticipated based on the values of the ternary end-members. Our results clearly demonstrate that alloying can allow both control of $T_t$ and enhancement of the BCE relative to the end-members, exploiting two different aspects of the transition.

## CONCLUSIONS

We have tailored large barocaloric effects at room temperature by alloying members of the $Mn_3(A,B)N$ antiperovskite series with (i) large transitional volume changes and (ii) transitions positioned either side of room temperature. We find a large entropy change at the 1st-order transition at 300 K in the material $Mn_3Zn_{0.5}In_{0.5}N$ and show that this is due to a large volume change relative to the sensitivity of the transition to pressure. Similarly to $Mn_3NiN$, a larger volume change occurs than expected when considering magnetovolume coupling alone, which is explained by the presence of multi-site magnetic exchange. The latter enhances the 1st-order behaviour and the barocaloric response relative to other materials with similar or larger spontaneous transitional volume changes, e.g. $Mn_3GaN$. Such a multi-site magnetic term in the free energy captures how the intrinsic geometrically frustrated AFM interactions strengthen with magnetic ordering, strongly stabilising the $\Gamma^{5g}$ AFM struc-

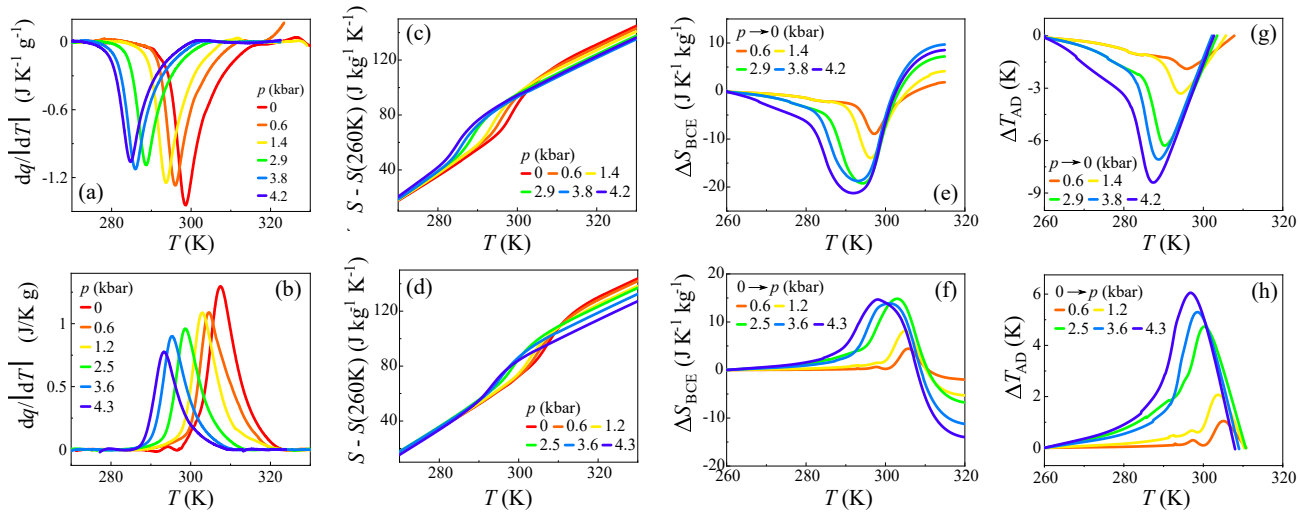


FIG. 3. Temperature dependent heat flow measurements measured on (a) cooling and (b) warming at various pressures; Isobaric entropy curves at different applied pressures on (c) cooling and (d) warming, extracted from the data in (a) and (b), respectively; Isothermal entropy change under (e) removal or (f) application of different pressures (BCE); Adiabatic temperature change under (g) removal or (h) application of different pressures.

ture. Pressure dependent neutron diffraction measurements reveal a mixed AFM-PM phase that exists close to the transition, when driven by temperature or pressure, which evidences the 1st-order nature of the transition. Our results further demonstrate the potential of quaternary alloying, opening up a vast phase space to explore $Mn_3(A,B)N$ for barocalorics and many other areas where these materials are being considered important for applications, such as spintronics [25, 26], strain-driven caloric cooling in thin films [21] and energy conversion [27].

We thank A.S. Wills for help with sample preparation. This work was supported by EPSRC (UK) grants (EP/P511109/1, EP/P030548/1, EP/J06750/1 and EP/M028941/1), MINECO project no. FIS2014-54734-P and ERC Starting grant no. 680032. D.B. is grateful for support from a Leverhulme Trust Early Career Fellowship (No. ECF-2019–351) and a University of Glasgow Lord Kelvin Adam Smith Fellowship. X.M. is grateful for support from the Royal Society.

* Corrsponding author: david.boldrin@glasgow.ac.uk

[1] B. Nair, T. Usui, S. Crossley, S. Kurdi, G. G. Guzmán-Verri, X. Moya, S. Hirose, and N. D. Mathur, Large electrocaloric effects in oxide multilayer capacitors over a wide temperature range, Nature **575**, 468 (2019).

[2] L. Mañosa and A. Planes, Materials with Giant Mechanocaloric Effects: Cooling by Strength, Advanced Materials **29**, 1603607 (2017).

[3] X. Moya, S. Kar-Narayan, and N. D. Mathur, Caloric materials near ferroic phase transitions, Nature Materials **13**, 439 (2014).

[4] J. Tušek, K. Engelbrecht, D. Eriksen, S. Dall'Olio, J. Tušek, and N. Pryds, A regenerative elastocaloric heat pump, Nature Energy **1**, 16134 (2016).

[5] P. Lloveras, A. Aznar, M. Barrio, P. Negrier, C. Popescu, A. Planes, L. Mañosa, E. Stern-Taulats, A. Avramenko, N. D. Mathur, X. Moya, and J.-L. Tamarit, Colossal barocaloric effects near room temperature in plastic crystals of neopentylglycol, Nature Communications **10**, 1803 (2019), arXiv:1903.12010.

[6] B. Li, Y. Kawakita, S. Ohira-Kawamura, T. Sugahara, H. Wang, J. Wang, Y. Chen, S. I. Kawaguchi, S. Kawaguchi, K. Ohara, K. Li, D. Yu, R. Mole, T. Hattori, T. Kikuchi, S.-i. Yano, Z. Zhang, Z. Zhang, W. Ren, S. Lin, O. Sakata, K. Nakajima, and Z. Zhang, Colossal barocaloric effects in plastic crystals, Nature **567**, 506 (2019).

[7] X. Moya, A. Avramenko, L. Mañosa, J.-L. Tamarit, and P. Lloveras, Use of Barocaloric Materials and Barocaloric Devices (2017).

[8] E. O. Chi, W. S. Kim, and N. H. Hur, Nearly Zero Temperature Coefficient of Resistivity in Antiperovskite Compound CuNMn$_{3}$, Solid State Communications **120**, 307 (2001).

[9] K. Takenaka, M. Ichigo, T. Hamada, A. Ozawa, T. Shibayama, T. Inagaki, and K. Asano, Magnetovolume Effects in Manganese Nitrides with Antiperovskite Structure, Science and Technology of Advanced Materials **15**, 15009 (2014).

[10] D. Boldrin, E. Mendive-Tapia, J. Zemen, J. B. Staunton, T. Hansen, A. Aznar, J.-L. Tamarit, M. Barrio, P. Lloveras, J. Kim, X. Moya, and L. F. Cohen, Multisite Exchange-Enhanced Barocaloric Response in Mn3NiN, Physical Review X **8**, 041035 (2018).

[11] D. Matsunami, A. Fujita, K. Takenaka, and M. Kano, Giant Barocaloric Effect Enhanced by the Frustration of the Antiferromagnetic Phase in Mn$_{3}$GaN, Nature Materials **14**, 73 (2014).

[12] D. Boldrin and L. F. Cohen, The role of competing magnetic interactions on the abnormal expansion properties in manganese antiperovskites, Mn$_{3+x}$A$_{1-x}$N (A = Ni, Sn), Journal of Alloys and Compounds **699**, 887 (2017).

[13] M. Rotter, H. Müller, E. Gratz, M. Doerr, and M. Loewenhaupt, A miniature capacitance dilatometer for magnetostriction and thermal expansion measurements, Review of Scientific Instruments **69**, 2742 (1998).

[14] J. Rodriguez-Carvajal, Recent advances in magnetic structure determination neutron powder diffraction, Physica B **192**, 55 (1993).

[15] B. H. Toby and R. B. Von Dreele, GSAS-II: The genesis of a modern open-source all purpose crystallography software package, Journal of Applied Crystallography **46**, 544 (2013).

[16] D. Fruchart and E. F. Bertaut, Magnetic Studies of the Metallic Perovskite-Type Compounds of Manganese, Journal of the Physical Society of Japan **44**, 781 (1978).

[17] D. Fruchart, E. F. Bertaut, R. Madar, and R. Fruchart, Diffraction Neutronique de Mn$_{3}$ZnN, Le Journal de Physique Colloques **32**, 876 (1971).

[18] *Landolt-Bornstein - New Series III/19c* (Springer-Verlag, 1981).

[19] C. Bean and D. Rodbell, Magnetic Disorder at a First Order Phase Transformation, Physical Review **126**, 104 (1962).

[20] E. Mendive-Tapia and J. B. Staunton, Ab initio theory of the Gibbs free energy and a hierarchy of local moment correlation functions in itinerant electron systems: The magnetism of the Mn3A materials class, Physical Review B **99**, 144424 (2019).

[21] J. Zemen, E. Mendive-Tapia, Z. Gercsi, R. Banerjee, J. B. Staunton, and K. G. Sandeman, Frustrated Magnetism and Caloric Effects in Mn-Based Antiperovskite Nitrides: Ab Initio Theory, Physical Review B **95**, 184438 (2017).

[22] E. Mendive-Tapia and J. B. Staunton, Theory of Magnetic Ordering in the Heavy Rare Earths: Ab Initio Electronic Origin of Pair- and Four-Spin Interactions, Physical Review Letters **118**, 197202 (2017).

[23] B. L. Gyorffy, A. J. Pindor, J. Staunton, G. M. Stocks, and H. Winter, A first-principles theory of ferromagnetic phase transitions in metals, Journal of Physics F: Metal Physics **15**, 1337 (1985).

[24] J. García, R. Navarro, J. Bartolomé, R. Burriel, D. González, and D. Fruchart, Specific heat of the cubic metallic perovskites Mn3ZnN and Mn3GaN, Journal of Magnetism and Magnetic Materials **15-18**, 1155 (1980).

[25] J. Zemen, Z. Gercsi, and K. G. Sandeman, Piezomagnetic Effect as a Counterpart of Negative Thermal Expansion in Magnetically Frustrated Mn-Based Antiperovskite Nitrides, Physical Review B **96**, 024451 (2017).

[26] D. Boldrin, I. Samathrakis, J. Zemen, A. Mihai, B. Zou, F. Johnson, B. D. Esser, D. W. McComb, P. K. Petrov, H. Zhang, and L. F. Cohen, Anomalous Hall effect in noncollinear antiferromagnetic Mn3NiN thin films, Physical Review Materials **3**, 094409 (2019), arXiv:1902.04357.

[27] X. Zhou, J.-P. Hanke, W. Feng, S. Bluegel, Y. Mokrousov, and Y. Yao, Giant Anomalous Nernst Effect in Noncollinear Antiferromagnetic Mn-based Antiperovskite Nitrides, Physical Review Materials **4**, 024408 (2020), arXiv:1908.11183.